SDSS'Rio 2010 STABILITY AND DUCTILITY OF STEEL STRUCTURES
Nobutaka Shimizu *et al.* (Eds.)
Rio de Janeiro, Brazil, September 8 - 10, 2010

STRENGTH ESTIMATION OF END FAILURES IN CORRUGATED STEEL SHEAR DIAPHRAGMS

Nobutaka Shimizu*, Kikuo Ikarashi**

* Nippon Steel Corporation
e-mail: shimizu.nobutaka@nsc.co.jp

** Tokyo Institute of Technology
e-mail: ikarashi.k.aa@m.titech.ac.jp

Keywords: Corrugated Steel Sheet, Diaphragm, Shear Strength, End Failure.

Abstract. *Shear tests on corrugated steel sheets were carried out to examine the effects of shape and thickness of profiles on the end failure action in lateral sway that may occur at the ends of flutes in shear diaphragms. Based on the test results, the previous shear deformation model for stiffness estimation was reviewed, and the deformation model was developed into a new shear strength model with application of yield-line hinges. The strength design formula was derived from the strength model through a limit analysis technique. Comparison with the test results showed that the derived formula provided appropriate strength estimation.*

1 INTRODUCTION

Structural design methods for corrugated steel sheets under in-plane shear force are systematized as "diaphragm design" and summarized in guidelines such as ECCS [1] and SDI [2]. These design guidelines allow rational structural systems, such as roof decks that resist shear force due to wind pressure or seismic loading without an additional bracing structure. In the structural design, global and local buckling of sheets, failure at the seam between sheets, and failure in sheet-to-frame fasteners are commonly estimated. Besides these failure modes, end failures, which may occur at the ends of flutes in corrugated shear diaphragms, are occasionally critical in deeper roof decks.

To use deeper decks as shear diaphragms as shown in Fig. 1a, Davies [3] proposed the strength design formula of end failures based on test results, in which the ends of flutes failed in lateral sway mode (Fig. 1b) or in web crippling mode (Fig. 1c). But the formula leans to give too conservative estimation especially for lateral sway, because the formula uses a factor based on test results in which almost all the specimens failed in web crippling mode.

In this study, end failure actions in lateral sway are examined through shear panel tests, and the effects of shape and thickness of profiles on lateral sway actions are clarified. Based on the test results, the previous shear deformation model for stiffness estimation is developed into a yield mechanics model for strength estimation. The strength design formula is derived from the model to improve the precision of strength estimation for deeper roof decks where end failure in lateral sway can occur.

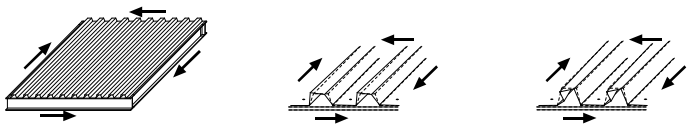

(a) Shear diaphragm (b) Lateral sway (c) Web crippling

Figure 1: End failure in a corrugated steel shear diaphragm

2 PREVIOUS STRENGTH DESIGN FORMULA OF END FAILURE

Davies [3] proposed a strength formula of end failure based on shear diaphragm tests with actual deeper roof decks. Figure 2 expresses the relationships between the shape of the profile and the end failure mode of each specimen, in which specimens with fastener failure are excluded. The horizontal axis in Fig. 2 indicates the ratio of profile-height h to profile-pitch q, and the vertical axis indicates the ratio of profile-height h to profile-thickness t. The circles represent lateral sway, and the triangles represent web crippling. Specimens of Davies' study are plotted with open symbols, and in this study, they are plotted with closed symbols. Figure 2 shows that many specimens of Davies' test collapsed in web crippling, and this trend is clearer in the range of h/t over 100 and h/q over 0.5.

Although Davies investigated theoretical approaches to lateral sway mode and web crippling mode, identical strength design formula ${}_cP_0$ was finally applied for both end failure modes as follows:

$$ {}_cP_0 = \alpha \cdot \sigma_y \cdot t^{1.5} \cdot b/q^{0.5} \tag{1} $$

where σ_y is the yield stress of the profile material, b is the length of the diaphragm, and α is a non-dimensional factor defined as 0.5 in reference [3] and as 0.9 in reference [1] to give conservative strength estimation for the profiles fastened to the frame in every trough of corrugation.

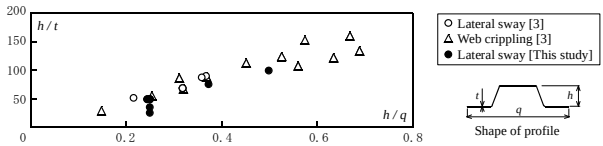

Figure 2: Relationship between profile shape and failure mode

3 SHEAR DIAPHRAGM TESTS

3.1 Outline of tests

The end failure actions of corrugated steel sheets with various shapes of profile were investigated by shear diaphragm tests using the setup shown in Fig. 3a. Every taught of the sheets was connected by a bolt (M6) on a steel frame (Fig. 3b) to make a friction-bolted joint. Static-monotonous shear force P was loaded to the frame by a hydraulic cylinder, and shear deformation δ was measured.

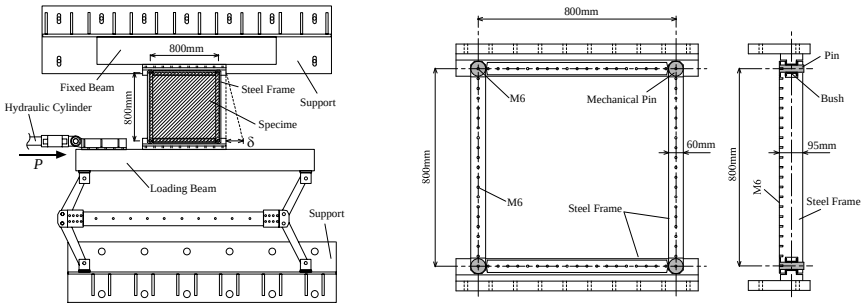

(a) Loading system (b) Steel frame

Figure 3: Test setup

The test specimens were corrugated steel sheets defined by the shapes according to the size symbols shown in Fig. 4a: a is the width of the diaphragm, b is the length of the diaphragm, q is the pitch of the

profile, h is the height of the profile, t is the thickness of the profile, e is half of the lower flange width, f is the upper flange width, g is the web projection width, and l is addition of the upper flange width and the web projection width. The sheets were bolted on the frame with a washer, whose width was j as shown in Fig. 4b, to secure a friction surface. A bolted connection is adopted to avoid connection failures, and a sheet without seams is used to avoid seam fastener failures in this test.

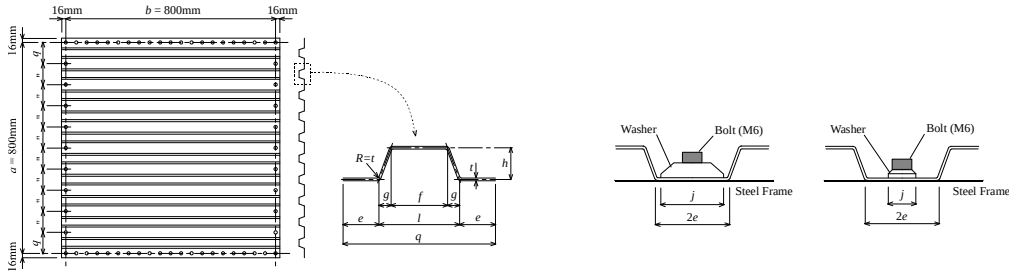

(a) Diaphragm size and shape of profile (b) Connection between sheet and frame

Figure 4: Specimen

Table 1 shows a list of the test parameters. The aim of Series I is to identify the effect of the shape of the profile: the upper flange width f, the height of profile h, and the thickness of profile t. The aim of Series II is to identify the effect of the width of washer j. Typical shapes of the specimens, like t04-h20-25 or t04-h20-f32, correspond with one-third scale roof deck in Japan. As shown in Fig. 2, profile shape ratios h/t and h/q for this test lie in the range of 25–100 and 0.25–0.5, respectively.

Table 1: Test parameters

Series	Specimen name	a (mm)	b (mm)	t (mm)	q (mm)	f (mm)	e (mm)	g (mm)	h (mm)	l (mm)	$2e$ (mm)	j (mm)
I	t04-h20-f40	800	800	0.4	80	40	20	0.0	20	40	40	34
	t04-h20-f25	800	800	0.4	80	25	20	7.5	20	40	40	34
	t04-h20-f15	800	800	0.4	80	15	20	12.5	20	40	40	34
	t04-h20-f0	800	800	0.4	80	0	20	20	20	40	40	34
	t04-h30-f25	800	800	0.4	80	25	20	7.5	30	40	40	34
	t04-h40-f25	800	800	0.4	80	25	20	7.5	40	40	40	34
	t06-h20-f25	800	800	0.6	80	25	20	7.5	20	40	40	34
	t08-h20-f25	800	800	0.8	80	25	20	7.5	20	40	40	34
II	t04-h20-f32	800	800	0.4	80	31.6	15.8	8.4	19.6	48.4	31.6	28
	t04-h20-f32J	800	800	0.4	80	31.6	15.8	8.4	19.6	48.4	31.6	12

The steel plates used for fabrication of the specimens are common between Series I and II, and their mechanical properties are shown in Table 2.

Table 2: Mechanical properties of steel plates

Thickness(mm)		Yield strength	Tensile strength	Elongation
Nominal	Measured	(N/mm^2)	(N/mm^2)	(%)
0.4	0.41	267	366	37.9
0.6	0.58	277	373	38.4
0.8	0.77	251	353	41.2

3.2 Test results

Almost all the specimens deformed elastically under shear force with elastic distortion of the flute cross sections at initial loading, and as shown in Fig. 5a, the distortion then moved to plastic end failure action

with lateral sway, which determines the ultimate strength. Viewed from a vertical angle as shown in Fig. 5b, every flute deformed linearly along the ridge lines and symmetrically around the center point of the upper flange. Therefore, the distortional deformation of the cross sections linearly decreased as they approached the centerline of the diaphragm length (A-A' section).

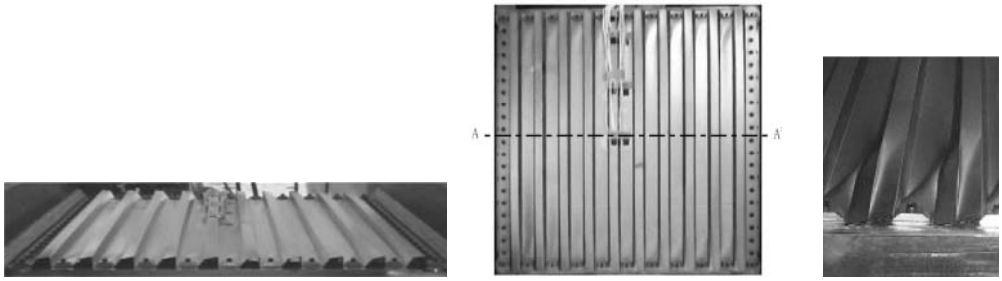

(a) Lateral sway in a horizontal angle (b) Lateral sway in a vertical angle (c) After lateral sway

Figure 5: Observation of end failure (t04-h20-f25)

Load-deformation (P-δ) relationships for all the specimens are shown in Fig. 6. After showing linear deformation behavior during the early loading stage, almost all the specimens showed gradual yielding and reached the ultimate strength determined by end failure in lateral sway. When loading advanced further from the status of Fig. 5a and 5b, the lateral sway changed into web crippling at the inclining sides; furthermore, the local tension field action mode of the steel plate around the bolted connection as shown in Fig. 5c, so that the specimens maintained strength in the load-decreasing range after reaching the ultimate strength.

The experimental values shown in Table 3 are obtained by the definition in Fig. 6e: The initial stiffness ${}_eK$ is defined as secant rigidity at shear deformation angle 1/800, the ultimate strength ${}_eP_u$ is defined as the maximum strength determined by lateral sway, and the yield strength ${}_eP_y$ is defined as the load corresponding to displacement of the intersecting point between a line drawn parallel to the horizontal axis passing through the point of ${}_eP_u$ and a line indicating ${}_eK$.

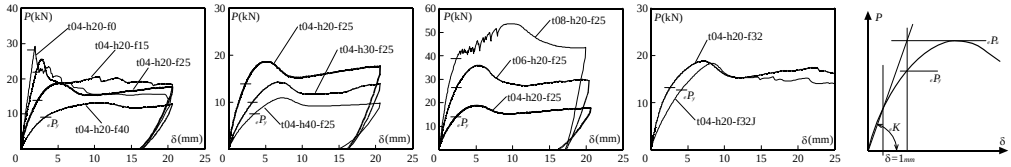

(a) Upper flange f (b) Height h (c) Thickness t (d) Washer j (e) Definition

Figure 6: Load-deformation (P-δ) relationship

Figure 6 shows that obvious differences due to the effect of the test parameters were identified in the initial stiffness, the yield strength, the ultimate strength, and load reduction after reaching ultimate strength. Furthermore, the P-δ relationship of t08-h20-f25 shows fluctuation of the load because of slip action in the friction-bolted connections.

Figure 6 and Table 3 show the effects of the experimental parameters as follows:

Effect of upper flange width f (Fig. 6a): The narrower the upper flange width is, the more the initial stiffness increases. The yield and ultimate strength rise as the upper flange width decreases, but the ultimate strength shows a slight difference between a width of 15 mm and a width of 0 mm. Furthermore, the load reduction tends to be rapid as the ultimate strength becomes higher.

Effect of profile height *h* (Fig. 6b): The higher the profile height is, the more the initial stiffness decreases. The yield and ultimate strength decrease as the profile height increases. In addition, the load reduction tends to be moderate as the ultimate strength becomes lower.
Effect of plate thickness *t* (Fig. 6c): The thicker the plate thickness is, the more the initial stiffness increases. The yield and ultimate strength rise as the thickness increases. Additionally, the load reduction tends to be somewhat rapid as the ultimate strength becomes higher.
Effect of the washer width *j* (Fig. 6d): The larger the washer width is, the more the initial stiffness increases, while there is no evident difference in the yield and ultimate strength as the washer width increases.

4 STRENGTH ESTIMATION OF END FAILURES IN LATERAL SWAY

4.1 Stiffness formula of distortional deformation

The previous stiffness formula of the corrugated shear diaphragms is reviewed to develop its deformation model into a strength model for a strength formula of end failure in lateral sway. When corrugated sheets receive shear force, distortional deformation of the flute of the cross section, as well as in-plane shear deformation of the plate elements, causes deformation of shear diaphragms. This distortional action is modeled as the deformed mechanics shown in Fig. 7a by Davies [4], in which it is assumed that the cross section receives bending moment and deforms linearly along the ridge lines and symmetrically around the center point of the upper flange. Based on equilibrium between the internal energy of the deformed mechanics and the external energy produced by the shear force, shear stiffness ${}_dK$ for the distortional deformation is obtained as follows:

$$ {}_dK = \frac{E \cdot t^3 \cdot b^3}{144D \cdot h^3 \cdot f^2} \tag{2} $$

where E is Young's modulus and D is the factor of the profile shape that is expressed in following equation:

$$ D = \frac{8e^3 + 8e^2 \cdot w - 4e \cdot f \cdot w + 2f^2 \cdot w + f^3}{12h(l+2e)^2} \tag{3} $$

Then, shear stiffness ${}_sK$ for in-plane shear deformation of the plate elements is given by the following equation:

$$ {}_sK = \frac{b \cdot t \cdot E}{2(f + 2w + 2e)(1+\nu)} \tag{4} $$

where ν is Poisson's ratio. Using stiffness values ${}_dK$ and ${}_sK$ per flute, the estimation formula of shear stiffness ${}_cK$ of the corrugated steel diaphragm, which has n number of flutes, is obtained as follows:

$$ {}_cK = \left(\frac{1}{{}_dK} + \frac{1}{{}_sK} \right)^{-1} \frac{1}{n} \tag{5} $$

4.2 Strength formula of end failure in lateral sway

The yield mechanics model shown in Fig. 7b is assumed by defining the yield-line hinges on the ridge lines of the profile, at which the bending moment of the cross section is maximized in the deformed mechanics model shown in Fig. 7a. The yield mechanics model, as well as the deformed mechanics model, is symmetrical around the center point of the upper flange. A new strength formula is derived from equilibrium between internal energy ${}_cU_i$ absorbed in the yield-line hinges and external energy ${}_cU_e$

produced by shear force ${}_cP$ and shear deformation ${}_c\delta$. In calculating the internal energy, the steel plate is considered to have the material properties of rigid plastic on the basis of the limit analysis technique.

The internal energy ${}_cU_i$ is given by plastic moment per unit length m_p $(=t^2\cdot\sigma_y/4)$ and the hinge rotation angles of web θ^w and upper flange θ^f at both ends of diaphragm length b as Equation (6), considering the geometrical condition of the mechanics whereby the hinge rotation angles linearly vary so as to fall to zero at the center of diaphragm length in which no cross section deformation occurs.

$$ {}_cU_i = m_p(4\theta^w + 2\theta^f)\frac{b}{2} \tag{6}$$

θ^w and θ^f are associated in Equation (7) considering displacement difference v between both ends on the upper flange and the continuous web.

$$ v = f\cdot\theta^f = 2w\cdot\theta^w\cdot\cos\phi \tag{7}$$

${}_cU_i$ is obtained by substituting Equation (7) for Equation (6) as follows:

$$ {}_cU_i = 4m_p\left(1+\frac{w}{f}\cos\phi\right)\theta^w\cdot\frac{b}{2} \tag{8}$$

Moreover, ${}_c\delta$ and θ^w are associated by the assumption that the upper flange rotates as a rigid body, so that the external energy ${}_cU_e$ is given as follows:

$$ {}_cU_e = {}_cP\cdot{}_c\delta = 2f\cdot w\cdot\theta^w\cdot\sin\phi/b\cdot{}_cP \tag{9}$$

Consequently, ${}_cP$ is obtained from the equilibrium between ${}_cU_i$ and ${}_cU_e$ as follows, corresponding to ultimate strength ${}_cP_u$:

$$ {}_cP = \frac{b^2}{f\cdot w\cdot\sin\phi}\left(1+\frac{w}{f}\cos\phi\right)m_p = {}_cP_u \tag{10}$$

In addition, yield strength ${}_cP_y$ is given by replacing the plastic moment m_p in Equation (10) with yield moment m_y $(=t^2\cdot\sigma_y/6)$ as follows:

$$ {}_cP_y = \frac{b^2}{f\cdot w\cdot\sin\varphi}\left(1+\frac{w}{f}\cos\phi\right)m_y \tag{11}$$

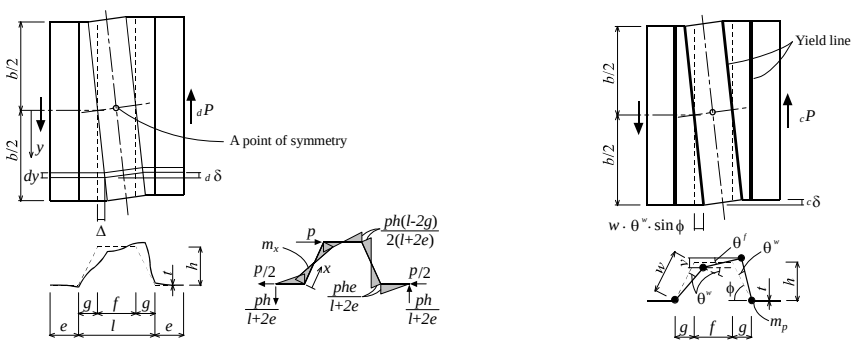

(a) Assumed deformed mechanics (b) Assumed yield mechanics

Figure 7: Estimation model

4.3 Correspondence between test results and formulas

Table 3 shows a comparison between test values ($_eK$, $_eP_y$, and $_eP_u$) and calculated values ($_cK$, $_cP_y$, $_cP_u$, and $_cP_0$ with α=0.9). Figure 8 and Fig. 9 indicate the relationships between the profile shape and the estimation result for stiffness and strength, respectively, for Series I. In these figures, the closed diamond, the closed square, and the closed circle indicate $_eK$, $_eP_y$, and $_eP_u$, respectively, and the open diamond, the open square, the open circle, and the open triangle indicate $_cK$, $_cP_y$, $_cP_u$, and $_cP_0$, respectively.

Figure 8 shows that the previous stiffness formula $_cK$ can provide appropriate estimation of the experimental initial stiffness $_eK$ when the profile shape varies, excluding the specimen with the upper flange width set to zero (t04-h20-f0). Furthermore, Figure 9 shows that the previous strength formula $_cP_0$ has low sensibility toward the test parameters and provides too conservative estimation of the experimental yield and ultimate strength ($_eP_y$ and $_eP_u$). By contrast, the proposed strength formulas $_cP_y$ and $_cP_u$ have favorable sensibility toward the test parameters and provide better estimation of $_eP_y$ and $_eP_u$ than of $_cP_0$.

Regarding Series II, Table 3 shows that calculated values give suitable estimation for the test results, but the specimens with small washer width (t04-h20-f32J) tend to give slightly higher calculated stiffness $_cK$ than experimental stiffness $_eK$.

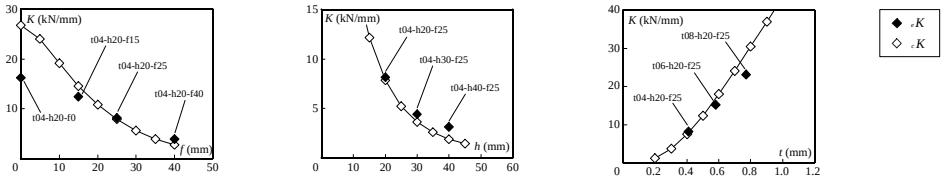

(a) Upper flange *f* (b) Height *h* (c) Thickness *t*

Figure 8: Estimation of stiffness

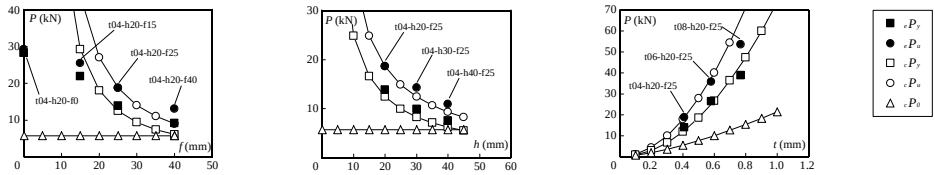

(a) Upper flange *f* (b) Height *h* (c) Thickness *t*

Figure 9: Estimation of strength

Table 3: Comparison between test result and calculation

Name		Test result			Calculation				Test result / Calculation				
		$_eK$ (kN/mm)	$_eP_y$ (kN)	$_eP_u$ (kN)	$_cK$ (kN/mm)	$_cP_y$ (kN)	$_cP_u$ (kN)	$_cP_0$ (kN)	$\frac{_eK}{_cK}$	$\frac{_eP_y}{_cP_y}$	$\frac{_eP_y}{_cP_0}$	$\frac{_eP_u}{_cP_u}$	$\frac{_eP_u}{_cP_0}$
I	t04-h20-f40	3.93	9.1	13.1	2.74	5.98	8.98	5.64	1.43	1.52	1.62	1.46	2.32
	t04-h20-f25	8.17	13.9	18.7	7.86	12.4	18.7	5.64	1.04	1.11	2.45	1.00	3.31
	t04-h20-f15	12.4	21.9	25.5	14.6	29.3	43.9	5.64	0.85	0.75	3.88	0.58	4.51
	t04-h20-f0	16.2	28.2	29.2	26.8	-	-	5.64	0.61	-	5.00	-	5.18
	t04-h30-f25	4.42	10.0	14.3	3.63	8.3	12.4	5.64	1.22	1.20	1.77	1.15	2.53
	t04-h40-f25	3.14	7.5	10.9	1.92	6.22	9.34	5.64	1.64	1.21	1.33	1.17	1.93
	t06-h20-f25	15.1	26.4	35.8	16.8	25.8	38.8	9.85	0.90	1.02	2.68	0.92	3.63
	t08-h20-f25	23.1	38.8	53.7	28.5	41.3	61.9	13.7	0.81	0.94	2.84	0.87	3.93
II	t04-h20-f32	7.27	13.2	18.8	6.34	9.78	14.7	5.64	1.15	1.35	2.33	1.28	3.34
	t04-h20-f32J	4.47	12.7	18.4	6.34	9.78	14.7	5.64	0.71	1.30	2.25	1.25	3.26

The precision of estimation of stiffness and strength seems to be lower as the upper flange width f decreases because the deformed mechanics model and the yield mechanics model tend to be determined by not only bending moment across the section but also in-plane axis force due to truss action. Improving the estimation accuracy of the mechanics model controlled by the truss action is a problem to be solved hereafter. Furthermore, the effect of the ratio of profile-pitch q to diaphragm-length b, which may influence the bending action across the section, ought to be investigated.

5 CONCLUSION

The effects of shape and thickness of the profile on end failure in lateral sway were examined through shear diaphragm tests on corrugated steel sheets. Based on the test results, the previous shear stiffness formula was reviewed and developed into a strength formula for end failure in lateral sway. The conclusions and findings are summarized as follows:

1. Almost all the specimens deformed elastically under shear force with elastic distortion of the flute cross section at initial loading, and the distortion moved to plastic end failure action with lateral sway, in which every flute deformed linearly along the ridge lines and symmetrically around the center point of the upper flange. Obvious differences due to the effect of shape and thickness of the profile were identified in the initial stiffness, the yield strength, and the ultimate strength of end failure action with lateral sway.
2. Based on the test observation of end failure in lateral sway, the yield mechanics model is assumed by defining the yield-line hinges on the ridge line of the profile, at which the bending moment of the cross section is maximized in the previous deformed mechanics model. The strength formula was derived from equilibrium between the internal energy of the yield-line hinges and the external energy of the shear force using a limit analysis technique. Comparison between the test results and the formulas shows that the previous stiffness formula and the proposed strength formula provide appropriate estimation in contrast to the excessive conservativeness of the previous strength formula.
3. The precision of estimation of stiffness and strength tends to be lower as the upper flange width becomes smaller because the deformed mechanics and the yield mechanics tend to be determined by not only bending moment across the section but also in-plane axis force due to truss action. Improving the estimation accuracy of the resistance mechanism determined by both bending and truss action is a problem left for future study.

REFERENCES

[1] European Convention for Construction Steelwork (ECCS), *European Recommendations for the Application of Metal Sheeting acting as a Diaphragm*, 1995.

[2] Steel Deck Institute (SDI), *Diaphragm Design Manual Third Edition*, 2004.

[3] J.M. Davies, J. Fisher, *End failure in stressed skin diaphragms*, Proc. Instn Civ. Engrs, Part2, 275-293, 1987.

[4] J.M. Davies, R.M. Lawson, *The Shear Deformation of Profiled Metal Sheeting*, International Journal for Methods in Engineering, Vol.12, 1507-1541, 1978

[5] J.M. Davies, *A General Solution for the Shear Flexibility of Profiled Sheets. I & II*, Thin-Walled Structures 4, 41-68 and 141-161, 1986